Friction **12**(3): 462–473 (2024)
https://doi.org/10.1007/s40544-023-0773-3
ISSN 2223-7690
CN 10-1237/TH
RESEARCH ARTICLE

Investigation of electrostatically tunable adhesion and instability of flying head slider

Fan ZHANG[1], Yu WANG[1,*], Yueqiang HU[2], Mingquan ZHANG[1], Baotong LI[1]

[1] *School of Mechanical Engineering, Xi'an Jiaotong University, Xi'an 710049, China*

[2] *National Engineering Research Center for High Efficiency Grinding, College of Mechanical and Vehicle Engineering, Hunan University, Changsha 410082, China*

Received: 22 April 2022 / Revised: 01 October 2022 / Accepted: 30 April 2023

Abstract: The interfacial adhesion between microstructures is inevitable in a micro-electro-mechanical system (e.g., hard disk drive (HDD)), which may lead to complicated microtribodynamics problems. This research has investigated the effect of surface potential on the interfacial adhesion and microtribodynamics of the head–disk interface (HDI) in an HDD. A dynamic continuum surface force model, where the electrowetting is considered, is proposed to evaluate the interfacial interaction, and then employed into a two-degree-of-freedom (2DOF) model to theoretically analyze the potential influence mechanism on the microtribodynamics. The results confirm that the elimination of potential can effectively repress the adhesion retention, which is further proved by the measured slider response with a laser Doppler vibrometer (LDV). Moreover, the effect of the potential on the adhesion-induced instability is also analyzed through the phase portrait. It tells that the critical stable flying height can be lowered with the elimination of potential.

Keywords: electric field (EF); retention; instability; adhesion

1 Introduction

The annual production volume of global data has continually developed rapidly in recent years. As the most salient magnetic storage device, the hard disk drive (HDD) takes great responsibility for storing those fast-growing data. Nowadays, the areal density (AD) or the capacity has been increased beyond 2 $Tb{\cdot}in^{-2}$ [1]. One of the practical techniques to increase the AD is decreasing the physical clearance of the head–disk interface (HDI), which now has come into smaller than 1 nm [2, 3]. At such a near regime, the grievous bouncing vibration of slider is aroused when it flies over a high-speed spinning disk. Meanwhile, the possibility of collision between the head and disk also increases intensely due to so close spacing. The frequent collisions cause the friction and aggravate the wear of slider, which lead to a decrease in the read/write performance of HDDs. For those reasons, the slider's bouncing contact vibration becomes a critical issue for further decrease of flying height.

When the slider is touching down (TD; i.e., the slider comes into contact with the disk, as shown in Fig. 7), the instable bouncing vibration amplitude arises suddenly at a certain flying height, which is called the TD height. Once the slider retracts from the disk, called the take-off (TO) process (as also shown in Fig. 7), the instable bouncing vibration vanishes until a higher threshold of flying height compared with the TD process [4], and the threshold is named the TO height. This is a kind of hysteresis phenomenon, which delays the separation of head and disk. Ono et al. [5] observed the hysteresis experimentally by controlling the atmospheric pressure of a chamber to drop or raise the head gradually. And they obtain the

* Corresponding author: Yu WANG, E-mail: ywang95@xjtu.edu.cn

hysteresis, as seen in the experiment by a two-degree-of-freedom (2DOF) model. Yoon and Talke [6] also found the "pressure hysteresis" by analyzing the acoustic emission (AE) signals. With further research on this issue, many researchers found that the hysteresis phenomenon is associated with the adhesive interaction between the head and disk. Thornton and Bogy [7] explained the hysteresis by simulating the slider motion, which has considered the intermolecular force. Guo et al. [8] employed molecular dynamics to obtain the nano-mechanics of perfluoropolyether (PFPE) films, and they found that the stronger HDI interaction induces the hysteresis. The lubricant-induced hysteresis is also demonstrated by Liu et al. [9]. In recent years, many researchers have focused on the surface potential of the HDI. The friction of nonconducting materials on the slider [10, 11] and contact of conducting materials [12, 13] can accumulate the charge on the surfaces, which generates the electric field (EF).

As a kind of attractive force, the electrostatic force F_e is even larger than the van der Waals force when the slider is lower than a certain threshold [14]; it has great influence on slider motion, affecting some details of the vibration instability of the slider [15], and cannot be ignored. Wang et al. [11] found that the F_e influenced instability of the slider experimentally, and they discovered that the slider has a faster release rate when the EF was removed, i.e., the instable vibration vanished at a lower TO height. Rajauria et al. [16] numerically analyzed the electrostatically tunable adhesion in the HDI and demonstrated that the hysteresis is effectively removed by an external alternating current (AC) voltage. However, they have ignored the lubricant, which is significant for head–disk adhesion, and the spreading behavior of lubricant on the disk surface is also affected by the existence of the EF, called electrowetting.

In this paper, we first consider the electrowetting behavior on the HDI at the nanoscale to study the effect of potential on the microtribodynamics of a flying slider. To overcome the continuity adhesion problem during investigating the slider dynamic motion, based on the improved sub-boundary lubrication (ISBL) model, a dynamic continuum surface force model is developed, and then introduced into a 2DOF dynamic model to explore the influence of the EF on the slider vibration. By analyzing the results, we found the effective repression of external voltage on the slider adhesion retention. It is a promising way to enhance the slider flying stability and durability.

2 Theoretical model: Interaction between head and disk

2.1 Dynamic continuous adhesion contact model between HDI

The commercially used HDD is a kind of complex microelectromechanical system. The two pivotal components in the HDD are the disk and the head suspension assembly, which are responsible for storing and reading/writing data, respectively, as shown in Fig. 1(a). The read/write components are enlarged to show more detail, observing in Fig. 1(b). When the disk rotates, the head on the suspension assembly keeps afloat on it to read/write data. More specifically, what directly affects the read/write performance of HDDs is the HDI, as simplified in Fig. 1(c). As can be seen, the femto-sized slider is covered with diamond-like carbon (DLC) and flies on the high-speed rotating disk passively through the self-pressurized air. As for the disk, it utilizes the glass as the substrate, which is deposited by the magnetic medium. To protect the medium, it is also covered with DLC and coated with a PFPE film for good lubrication finally.

Since the slider contacts with the disk, the interaction between them lumps in a miniature region, where thermal-induced protrusion of head would contact with the disk, as sketched in Fig. 1(d). Due to the limitation of force effective range at the nanoscale, the force interaction is concentrated on the carbon (head)–lubricant–carbon (disk) interface, which is also our research interface. If there is no special instruction, the HDI mentioned below is the carbon–lubricant–carbon interface. Although both the realistic disk and head surfaces are rough, it is feasible to combine them into a smooth surface and a rough surface, and which one is selected has no influence on the mathematics [17]. According to the Greenwood and Williamson (GW) model [18], the disk is considered to be covered with a large number

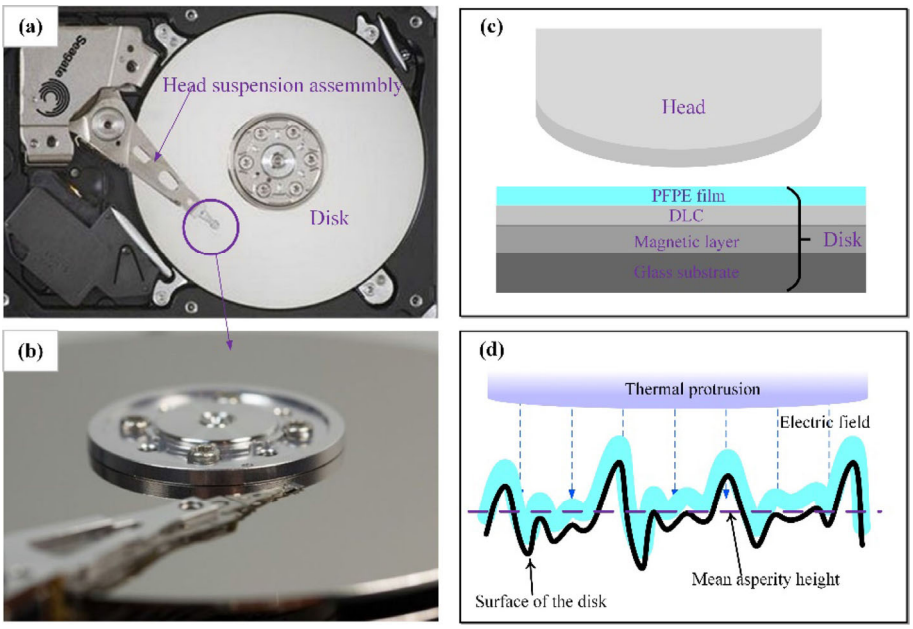

Fig. 1 (a) HDD, (b) enlarged graph of read/write components, (c) schematic diagram of composition of disk, and (d) schematic diagram of HDI.

of asperities, which are spheres with the same radius R_a, and whose height follows a Gaussian distribution, as shown in Fig. 2(a), with a mean height μ and a standard deviation σ. As for the lubricant, we assume that the PFPE film overcoats on the asperities evenly with a thickness t. For descriptive and computational reasons, taking the mean asperity height as a reference, the minimum spacing between the head protrusion and the reference is defined as the head separation d, and the height of the asperity is denoted by z.

At the nanoscale, the head is attracted by both the DLC and the lubricate of the disk because of the van der Waals force. When it gets closer to the disk and contact with the mobile lube, a liquid bridge is formed between the head smooth surface and the spherical asperities of the disk, which then leads to stronger adhesion attraction. Continuing to lower the head, it impacts with the DLC asperities. At this state, there exists adhesion between solid and solid except for liquid–solid adhesion. To evaluate the adhesive interaction of the HDI, we adopt a continuum mechanics-based adhesive model, called the ISBL model [19]. This rough surface adhesive model had adopted the similar idea of the sub-boundary lubrication (SBL) [20] model to extend the Kogut and Etsion (KE) model [21] to also contain the presence of a lubricant

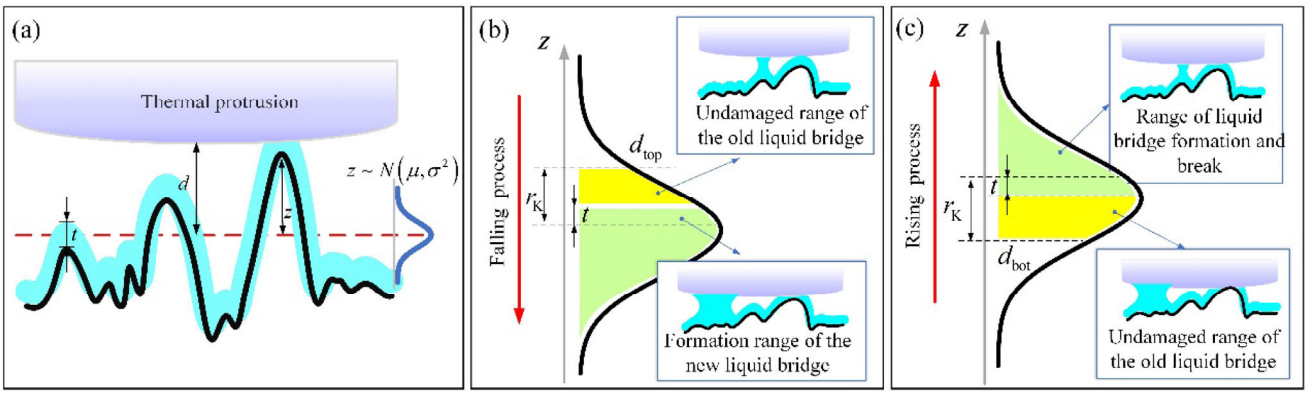

Fig. 2 (a) Gaussian distribution of asperity height, (b) interaction between lubricant and head during head falling, and (c) interaction between lubricant and head during head rising. Note: r_K is the Kelvin radius, and d_{top} and d_{bot} are the separation, at which the head is about to fall or rise (transition of changing direction) in the last up and down cycle, respectively.

film. Thus, this model has the ability to evaluate the contribution of a thin lubricant as part of the adhesion. The total adhesion force F_s calculated by the model is given by Eq. (1) [19]:

$$F_s = A_n \eta 2\pi R_a \Delta\gamma \left(\int_{-\infty}^{d-t} J_{nc} + \int_{d-t}^{d} J_{lc} + 0.98\int_{d}^{d+w_c} J_{-0.29}^{0.298} + 0.79\int_{d+w_c}^{d+6w_c} J_{-0.321}^{0.356} + 1.19\int_{d+6w_c}^{d+110w_c} J_{-0.332}^{0.093}\right) \quad (1)$$

where A_n is the nominal contact area, η is the density of asperities, $\Delta\gamma$ is the energy of adhesion, and ω_c is the critical interface at the inception of plastic deformation. The first integral J_{nc} represents the attractive effect of noncontact asperities on disk in Eq. (1), the second one J_{lc} is the lubricant-induced interaction, and the last three which follow the form J_c^b calculate the adhesion of the contact asperities. $A_n \eta 2\pi R_a \Delta\gamma$ is represent by a symbol ψ. In Ref. [22], the symbols J_{nc}, J_{lc} and J_c^b follow Eq. (2).

$$\begin{cases} J_{nc} = \dfrac{4}{3}\left[\left(\dfrac{z_0}{z_0 - w - t}\right)^2 - \dfrac{1}{4}\left(\dfrac{z_0}{z_0 - w - t}\right)^8\right]\phi(z)\mathrm{d}z \\ J_{lc} = \phi(z)\mathrm{d}z \\ J_c^b = \left(\dfrac{\omega}{\omega_c}\right)^b \left(\dfrac{z_0}{\omega_c}\right)^c \phi(z)\mathrm{d}z \end{cases} \quad (2)$$

where z_0 is the equilibrium spacing, and ω is the interference between the smooth surface and the asperity, i.e., the distance, which points outside the deforming zone move together during the deformation [18]. $\phi(z)$ represents the normalized Gaussian distribution of asperity height, and ω_c is defined as [23]:

$$\omega_c = \left(\frac{\pi K H}{2E^*}\right)^2 R_a \quad (3)$$

where H represents the hardness of the softer material, K is the hardness coefficient, which is also associated with the Poisson's ratio of the softer material, and E^* is the composite Young's modulus, which is related to the Young's moduli and Poisson's ratios of the contact surfaces.

At the contact state, the repulsion between HDIs also appears because of the deformation of those asperities, except for the attraction calculated by Eq. (1). The contact force F_c in the contact rough area can be calculated by Eq. (4) [23]:

$$F_c = \eta A_n \left\{\frac{4}{3} E^* R_a^{1/2} \int_d^{d+\omega_c} (z-d)^{1.5} \phi(z)\mathrm{d}z + \pi R_a K H \int_{d+\omega_c}^{+\infty} \left[2(z-d) - \omega_c\right]\phi(z)\mathrm{d}z\right\} \quad (4)$$

In this model, the elastic and the plastic deformation-induced F_c of those asperities are estimated by the first and the second integrals, respectively.

The HDI, a nano system composed of multi-material layers, tends to exist the electrical double layer force because of the potentials, which are caused by contact and friction (contact potential and tribocharging). Generally, it is considered that the electrostatic attraction comes from the charges on surface layers of only a few angstroms, while the effect from those beyond the surface layers is neglected [24]. Considering the rough surface in a statistical sense as the GW model did, this F_e calculation equation is written as [14]:

$$F_e = A_n \eta \pi \varepsilon_0 R_a U^2 \int_{-\infty}^{d-t} \frac{1}{d-t-z} \phi(z)\mathrm{d}z \quad (5)$$

where ε_0 is the permittivity of vacuum, and U is the interfacial potential between HDI.

When there is an EF in the HDI, the lubricant-induced adhesion needs to be renewed. Most researchers have found that the surface potential has the influence on the interfacial tension of the solid–liquid phase, called electrowetting. At this state, the contact angle θ of the liquid near the three-phase contact line decreases due to the electrostatic mechanics. Let us refocus on the second item of Eq. (1). The equivalent interface energy needs to be modified by introducing an item related to the potential; meanwhile, the modification contribution of line tension is also essential at the nanoscale. Wang and Zhao [25] established a uniform expression about electrowetting on dielectric including the line tension. So, we employ the equation to rewrite Eq. (1) in this paper, and the second integral term F_{slb} about the lubricant influence is given by Eqs. (6) and (7):

$$F_{slb} = \psi\left[C_e \int_{d-t}^{d} \left(1 - \frac{d-z}{2r_1 \cos\theta}\right)\phi(z)\mathrm{d}z\right] \quad (6)$$

$$C_e(U,\tau)=\frac{1}{\Delta\gamma}\left(\Delta\gamma\cos\theta+\frac{\varepsilon_0\varepsilon U^2}{2d_{ins}}-\frac{\tau}{R_a}\right) \tag{7}$$

where C_e is the correction factor of lubricant adhesion influenced by the interfacial potential, d_{ins} is the thickness of the insulator, which means DLC here, and r_1 is the mean curvature of the meniscus. ε is the permittivity of lubricant, and the last one, i.e., $\frac{\tau}{R_a}$, represents the influence of line tension τ.

Equation (6) is applicable to a quasi-static process; however, the sider oscillates on the rotating disk when it is working. From the experiment measure of pull-in and pull-off forces implemented by Tani et al. [26], the capillary adhesion also exists at the nanoscale. So, this lubricant adhesion difference should be considered in the dynamic model during falling and rising, i.e., the difference between the height of liquid bridge formation and the height of liquid bridge breaks. It assumes that the bridge starts to form when the protrusion contacts with the lubricant, which means that the formation separation between asperity and protrusion is t. As for the break separation of asperity and protrusion, it is $2r_1\cos\theta$ from Eq. (6). When the liquid bridge is at the equilibrium, the θ is constant so that the r_1 also keeps constant, which is equal to the Kelvin radius r_K. This is also the separation, at which the bridge finally disappears.

Besides, to ensure the calculation continuity of F_s when the head changes the direction, we proposed the following integration method. The separation, at which the head is about to fall or rise (transition of changing the direction) in the last up and down cycle, are defined as d_{top} and d_{hot}, respectively.

During the falling process, as shown in Fig. 2(b), if the slider disk spacing meets the range: $d_{top}-r_K+t\le d\le d_{top}$ (the yellow area in Fig. 2(b)), the lubricant adhesion is calculated by Eq. (8):

$$F_{slb}=\psi\left(C_e\int_{d_{top}-r_K}^{d}\left(1-\frac{d-z}{r_K}\right)\phi(z)\mathrm{d}z\right) \tag{8}$$

and if the spacing meets $d\le d_{top}-r_K+t$ (the green area in Fig. 2(b)),

$$F_{slb}=\psi\left(C_e\int_{d-t}^{d}\left(1-\frac{d-z}{r_K}\right)\phi(z)\mathrm{d}z\right) \tag{9}$$

During the rising process, as shown in Fig. 2(c), if the spacing meets $d_{bot}\le d\le d_{bot}+r_K-t$, the lubricant adhesion is calculated by Eq. (10):

$$F_{slb}=\psi\left[C_e\int_{d_{bot}-t}^{d}\left(1-\frac{d-z}{r_K}\right)\phi(z)\mathrm{d}z\right] \tag{10}$$

and if the spacing meets $d>d_{bot}+r_K-t$,

$$F_{slb}=\psi\left(C_e\int_{d-r_K}^{d}\left(1-\frac{d-z}{r_K}\right)\phi(z)\mathrm{d}z\right) \tag{11}$$

Then the F_s as a function of the head–disk gap is obtained via the proposed dynamic continuum surface force model, and the results are graphed in Fig. 3. The head descends from 6 nm above the disk until the gap is −2 nm; later, it suddenly rises to the distance of 5.5 nm. Then, another sudden decrease follows and continues the up–down cycle. Noticing the transition enclosed by those red circles, the values are continuous when the head changes its direction. However, it could jump to another value in the former adhesion numerical calculation model of Ref. [4] even everything about affecting the F_s has not changed at that time, which is against with the results of experiments and simulations [8, 26]. Here, the limitation is solved in our proposed model. And another attention is that the adhesion may be differential even when the head is at the same height and in the same up/down process. For example, when the head–disk gap is 2 nm and in the falling process, i.e., numbered with 1, 3, and 5, the F_s are different between them. This is the influence

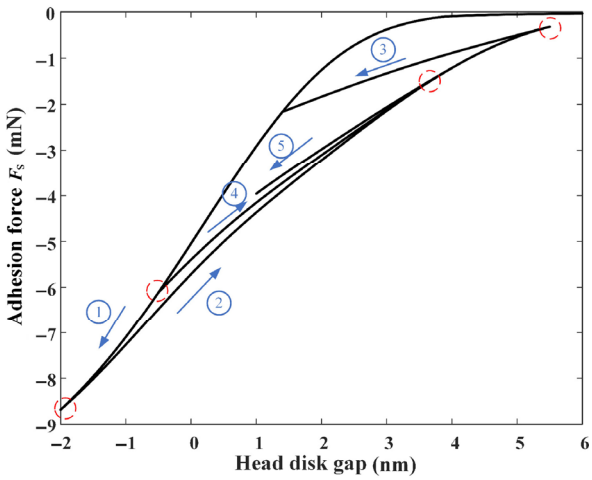

Fig. 3 Continuum F_s between head and disk when the head rises and falls.

of those asperities, whose lubricant bridge does not break at the transition.

2.2 Dynamics analysis of 2DOF model during TD/TO

To analyze the microtribodynamics of the slider on the real complex HDI, we expect to obtain the motion with a simplified model of the head–disk system. Due to the contact collision and friction between the head and disk, the vertical movement of the slider and the flip of the pitch direction are mainly influenced, as sketched in Fig. 4. Thus, a 2DOF dynamic model is established, as shown in Fig. 4.

In this model, the X axis is defined as the mean asperity height of the disk when calculating the interaction between the HDI, and the vertical line passing the centroid of the slider in the initial position is defined as the Z axis. The slider is simplified as a cuboid with mass m, pitch moment of inertia $\boldsymbol{J}$ about centroid, length a, and width b. It is flexibly connected with the folding arm, which can move horizontally along the Z axis or rotate around its own centroid, so the arm is represented by the ordinary spring damper (k and c) and torsion spring damper (k_θ and c_θ). Meanwhile, because the slider floats over the rotating disk due to the air flow, the flow can also be represented by a spring-damper system. The air bearing surface of the slider is an etched complexity surface that can influence the flip of the pitch direction, and thus the front and rear air bearing pad are divided in this system; they are represented by the front spring damper (k_f and c_f) and rear spring damper (k_r and c_r), respectively. The air forces are assumed to be acted on a point of the front and rear air bearing pad, and the horizontal distances from the point to the centroid of slider are defined as d_r and d_f. Again, the minimum spacing between the head protrusion and the X axis is denoted by d. The height from the X axis to the centroid of the slider under static state is defined as F_H.

As the small contact area between the protrusion of slider and the disk, we assume that those interaction (attraction, repulsion, and friction) lumps on the protrusion and the contact area do not change at any interference depth. So, those interaction forces can be calculated at any separation by the equations (Eqs. (1), (4), and (5) and Eqs. (8)–(11)) described in Section 2.1. The concentrated force F is calculated by $F_\mathrm{c}-F_\mathrm{s}-F_\mathrm{e}$. Meanwhile, the friction force Q exerted on the protrusion together with a concentrated force excites the slider rotation at the pitch direction, and the torque $\boldsymbol{M}$ except for the part caused by airflow applied on the slider is in Eq. (12).

$$\boldsymbol{M}=-0.5bQ+d_\mathrm{h}F \tag{12}$$

where d_h represents the distance from read/write head to the centroid of the slider.

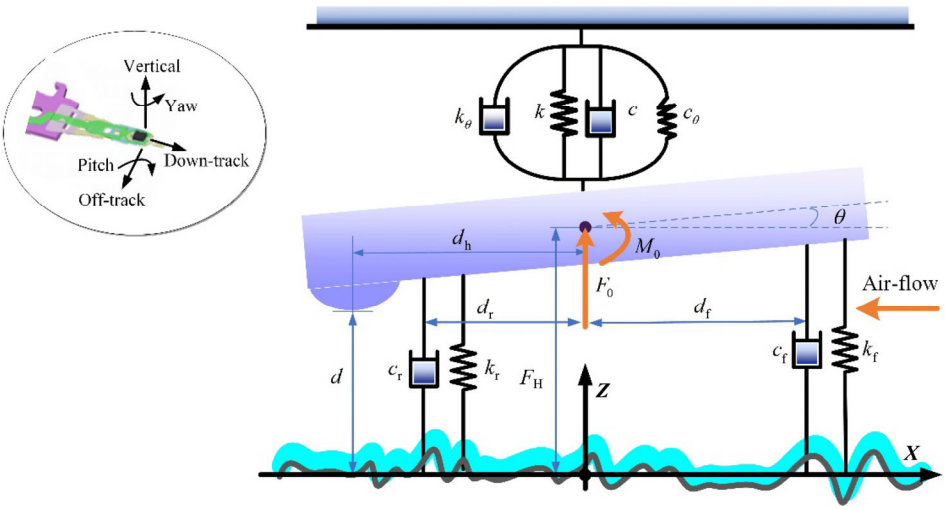

Fig. 4 Schematic diagram of simplified 2DOF dynamic model of HDI system. Note: X and Z represents axes, k and c are the ordinary spring damper, k_θ and c_θ are the torsion spring damper, k_f and c_f are the front spring damper, k_r and c_r are the rear spring damper, F_H is the height from the X axis to the centroid of the slider under static state, d_h represents the distance from read/write head to the centroid of the slider, and d_r and d_f are the horizontal distances from the point to the centroid of slider.

Because the friction law in microtribodynamics does not obey the common Coulomb friction law, the strength of bond where contact occurs and the shear during sliding [21] between slider and disk need to be involved. Thus, the Q is given by Eq. (13):

$$Q = \mu_{\mathrm{f}}(F_{\mathrm{c}} - F_{\mathrm{s}}) \tag{13}$$

where μ_{f} is the friction coefficient between the head and disk.

When we define the vertical displacement of the slider as z_{s} and the angular displacement in the pitch direction as θ, the motion of the slider can be expressed by Eq. (14):

$$\begin{bmatrix} m & 0 \\ 0 & J \end{bmatrix}\begin{Bmatrix} z_{\mathrm{s}}'' \\ \theta'' \end{Bmatrix} + \begin{bmatrix} C_{11} & C_{12} \\ C_{21} & C_{22} \end{bmatrix}\begin{Bmatrix} z_{\mathrm{s}}' \\ \theta' \end{Bmatrix} + \begin{bmatrix} K_{11} & K_{12} \\ K_{21} & K_{22} \end{bmatrix}\begin{Bmatrix} z_{\mathrm{s}} \\ \theta \end{Bmatrix} = \begin{Bmatrix} F \\ M \end{Bmatrix} \tag{14}$$

where the elements in the stiffness matrix K_{11}, K_{12}, K_{21}, and K_{22} can be obtained by Eq. (15):

$$\begin{aligned} K_{11} &= k_{\mathrm{f}} + k_{\mathrm{r}} + k \\ K_{12} &= k_{\mathrm{f}} d_{\mathrm{f}} + k_{\mathrm{r}} d_{\mathrm{r}} = K_{21} \\ K_{22} &= k_{\mathrm{f}} d_{\mathrm{f}}^2 + k_{\mathrm{r}} d_{\mathrm{r}}^2 + k_{\theta} \end{aligned} \tag{15}$$

And the elements in the damping matrix C_{11}, C_{12}, C_{21}, and C_{22} can be obtained by Eq. (16):

$$\begin{aligned} C_{11} &= c_{\mathrm{f}} + c_{\mathrm{r}} + c \\ C_{12} &= c_{\mathrm{f}} d_{\mathrm{f}} + c_{\mathrm{r}} d_{\mathrm{r}} = C_{21} \\ C_{22} &= c_{\mathrm{f}} d_{\mathrm{f}}^2 + c_{\mathrm{r}} d_{\mathrm{r}}^2 + c_{\theta} \end{aligned} \tag{16}$$

The damping coefficients c, c_{f}, c_{r}, and c_{θ} are calculated [27].

3 Experimental

Figure 5 presents the diagram of the slider TD/TO tests to explore the influence of the surface potential, which is eliminated by applying and external voltage between HDIs. The disk is driven by a spindle to float the slider through the high-speed rotating airflow. And the head suspension assembly is mounted at a certain height above the disk, whose position is controlled by the driver chained with the computer. The power of the TFC heater is also operated by the computer.

The AE sensor is glued to the arm of the head suspension assembly. It is adopted for the TD test since it is sensitive to the contact between the head and disk [28]. Then the TD power (TDP) of the TFC heater is obtained through the measured AE signal. To monitor the vibration of the slider, the LDV is employed, which is located directly above the head. The actual measuring points of both AE and LDV are shown inside the blue wireframe.

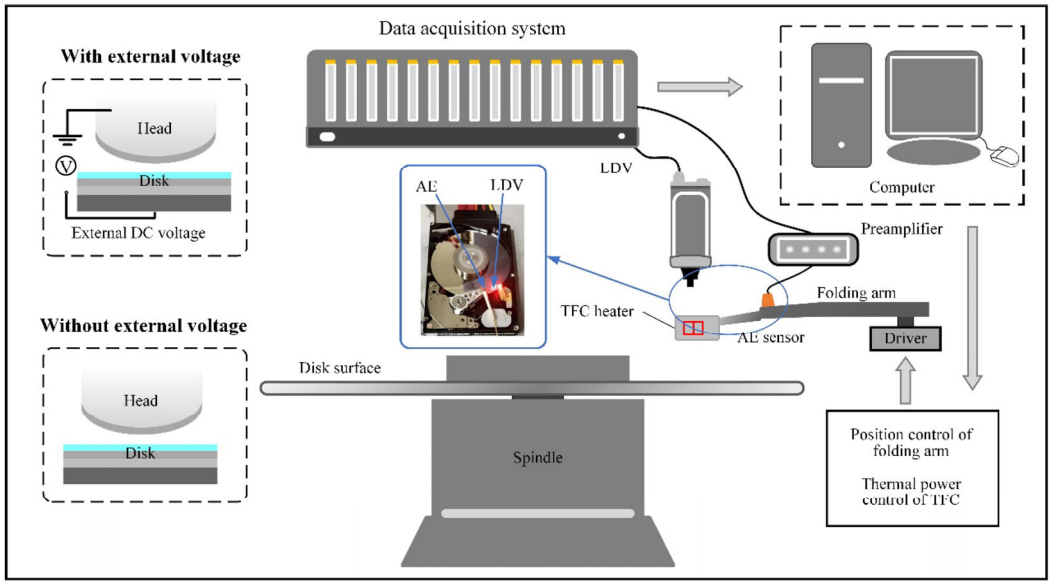

Fig. 5 Schematic of slider test setup. Note: DC is the abbreviation of direct current, and LDV is the abbreviation of laser Doppler vibrometer.

To investigate the effect of the potential-induced EF on the slider microtribodynamics, we apply an external voltage to eliminate the potential between HDIs, as schemed in the bottom left of Fig. 5. The vibration signal of the slider is collected in this case. And the vibration signal under the normal condition, i.e., without external voltage, is also acquired for comparison.

4 Results and discussion

4.1 Effect of potential on slider adhesion hysteresis during TD/TO

To investigate the effect of the potential between HDIs, we simulate the dynamic vibration response of TD/TO process, employing the introduced model in Section 2, and the results are illustrated in Fig. 6. It shows the slider vibration response without and with external voltage. The vibration results can be divided into three stages: flying, bouncing, and surfing exactly, as depicted in Fig. 6. The retention is obviously observed by comparing adhesion duration (duration of both bouncing and surfing stages) of the results. The duration (about 0.2–1.3 ms in Fig. 6(b)) of the adhesion state is shortened in the condition of applying 0.7 V of external voltage. It indicates that the adhesion retention is suppressed by removing the potential between HDIs by our simulation.

Later, we performed the TD/TO tests to verify the conclusion. With the commercially used femto head, the head changes its height at the nanoscale by controlling the TFC heater power. When the power increases, the protrusion gets nearer to the disk surface; contrarily, it is further from the disk gradually. During the tests, the vibration signal of the slider is measured by the LDV at each power step. To evaluate the influence of the EF between HDIs, we apply an external voltage to eliminate the original potential. However, before developing this operation, the "TD method" [29] is applied to determine the difference of potential (0.7 V) between slider and disk. Then, starting the TD/TO tests, the obtained signal is bandpass filtered since the frequencies of the pitch model and normal model are in the frequency band range from 50 to 300 kHz. In this way, we can better identify the dynamic characteristics of the head, and the results are depicted in Figs. 7(a) and 7(b), showing the dynamic vibration without and with the applying external voltage during TD/TO, respectively. As can be seen in Figs. 7(a) and 7(b), initially during the TD process, the slider vibrates with a limited modulation amplitude. Note that the vibration in the state seems to be zero in the simulation, but the experimental results are not. This is because the actual air bearing is variable stiffness, but it is a constant in the simulation. It is fine for the adhesion study as the previous studies did in this way [5, 15, 27]. Back to the topic, with the increase of heater power, the slider is pushed to touch down; it vibrates violently at a certain heater power value, and the vibration amplitude continues to increase as the heater power raises regardless of whether there is an external EF. However, the vibration would start to attenuate and tend to remain temporary stability if the power adds more. After a short while, the TO process starts as the power releases, and the measured slider vibration experience is similar to the opposite process of TD. As seen from the results, the duration of adhesion is shorted by eliminating the surface potential, which agrees with our simulation conclusion.

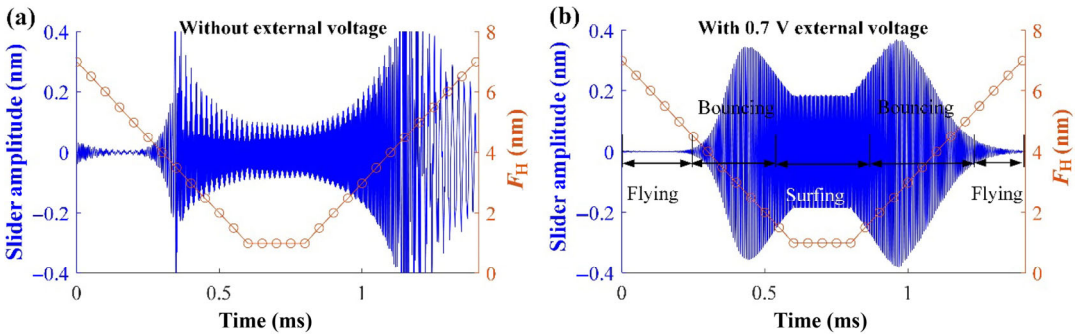

Fig. 6 Simulation results of slider response during TD/TO. (a) Vibration response of slider without external voltage and (b) vibration response of slider with 0.7 V of external voltage.

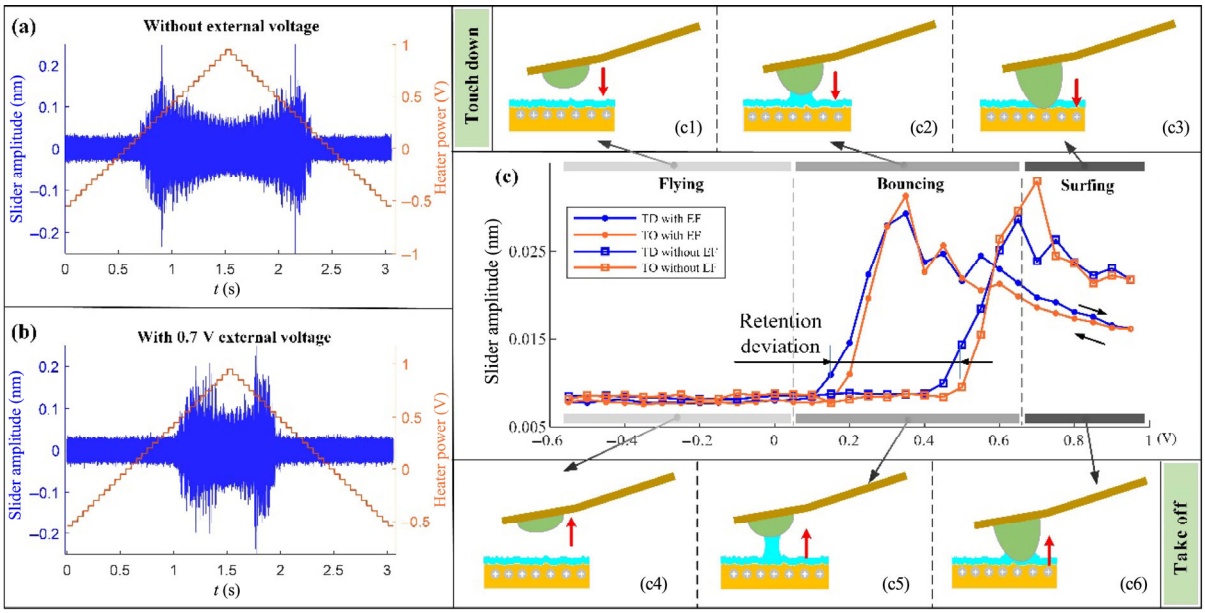

Fig. 7 Experimental results of slider response during TD/TO. (a) Vibration response of slider without external voltage, (b) vibration response of slider with 0.7 V of external voltage, and (c) root mean square (RMS) of slider vibration response in two cases: (c1–c3) schematic diagrams of slider TD process and (c4–c6) schematic diagrams of slider TO process.

To better understand the effect of the elimination of the potential, the RMS value of the vibration amplitude with and without the EF at each power step is calculated, and the change along with the power is sketched in Fig. 7(c) together. They are roughly divided into three movement stages as the simulation results: flying, bouncing, and surfing [30], where the slider vibrates slightly, bounces strongly, and oscillates stably. Taking the power of starting bouncing vibration as the critical stable flight criterion, i.e., equivalent to the TD height and TO height, there exists obvious adhesion retention deviation between the two cases. That is to say that the external voltage can suppress the adhesion interaction between the slider and the disk, which enables the slider to release the bouncing early.

4.2 Effect of potential on slider instability

As the critical stable flying height is important for the magnetic recording density, we are ready to discuss the effect of external voltage in Section 4.2. The RMS values of the slider simulation response during TO are calculated for each 0.05 ms. And the calculation results are compared for both the normal and external voltage application state, which are depicted in Figs. 8(a) and 8(c), respectively.

Figure 8(b) is the Gaussian distribution of the asperity height along with the F_H. Combined with the TD and TO process illustration, as shown in Figs. 7(c1)–7(c6), we can have a better understanding of slider instability. When $F_H = 1$ nm, the slider contacts with a large number of asperities, as shown in Fig. 7(c4). The slider vibrates slightly driven mainly by F_c and friction between head and disk, and the phase portrait of the slider vibration reveals that it is a self-excited vibration as its periodicity, as displayed by Fig. 8(c1). As the F_H increases, the amplitude of the vibration also increases, and those quasi-circular phase trajectories no longer coincide and gradually separate, as shown in Figs. 8(a1), 8(a2), and 8(c2). Then, with the continued increase of F_H, the phase trajectory is approaching the center as time goes by, and the head is far from the disk, which means that the influence of the rough disk surface is weakened, and the slider is in stable flying, as shown in Figs. 8(a3) and 8(c3). We can focus on that the F_H of the bouncing vibration is lower with applying an external voltage by comparing Figs. 8(a) and 8(c). Figure 8(a) shows that the slider starts to be instable even if the F_H does not touch the 3σ lubricant contact line. That is the results of the adsorption of lubricant and EF. With the elimination of surface potential, the adsorption

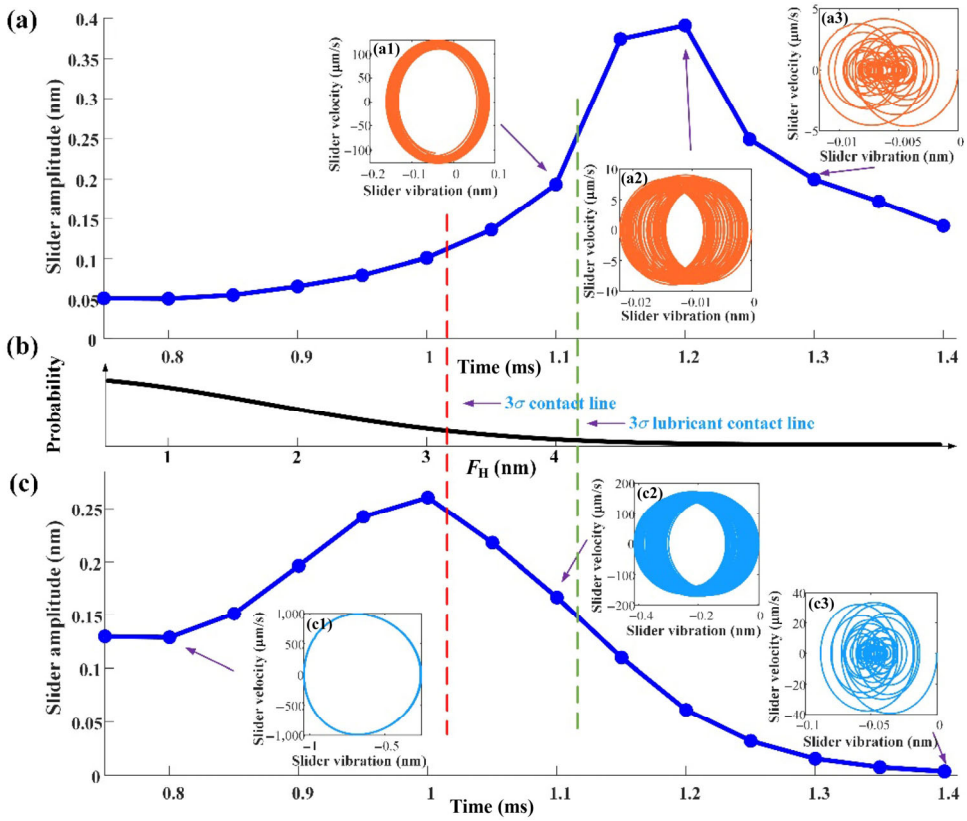

Fig. 8 (a) RMS of slider simulation response during TO without external voltage, (b) probability distribution of asperity height, and (c) RMS of slider simulation response during TO with external voltage.

is weakened, leading to the reduction of critical instability F_H. This proves that the stable flying height can be lower for a larger recording density. In Fig. 8, there is an explanation for the amplitude reduction of the surfing state. Due to the increased number of contact asperities, the F_c dominates the motion, and the contact stiffness enhances. The amplitude decreases, and the slider gradually comes into the amplitude steady state.

5 Conclusions

In this research, the effect of surface potential on the flying slider microtribodynamics has been investigated. A continuum surface force model is proposed to evaluate the interaction between the head and disk. And then, a 2DOF dynamic model is employed to study the influence mechanism of potential on slider microtribodynamics theoretically. We experimentally obtain the dynamic motion by the LDV without and with an applied external voltage of 0.7 V, which reveals that the simulation agrees well with the experiment. From the results of both simulation and experiment, we find that the adhesion retention can be suppressed by eliminating the surface potential, which might mean a less wear loss of the head. Besides, the critical stable flying height of the slider can be lowered in this way, which may lead to a larger recording density. The electrostatically tunable method provides a promising way to enhance the slider flying stability and durability.

Acknowledgements

The authors would like to thank the National Natural Science Foundation of China (Nos. 61633001 and 51875437) for the support in this research.

Declaration of competing interest

The authors have no competing interests to declare that are relevant to the content of this article.

References

[1] Saenphum N, Chureemart J, Evans R F L, Chantrell R W, Chureemart P. Large magnetoresistance in Heusler alloy-based current perpendicular to plane giant magnetoresistance sensors. *J Phys D Appl Phys* **54**(39): 395004 (2021)

[2] Yang A, Wang Y, Zi Y Y, Liang X H. Quantitative identification of slider nanoscale wear based on the head–disk interface dynamics. *Tribol Int* **116**: 95–104 (2017)

[3] Ono K. Numerical simulation of thermal fly-height control slider touchdown test for achieving ideal subnanometer clearance head slider touchdown behaviors. *Tribol Lett* **68**(1): 44 (2020)

[4] Ono K. Design considerations of a contact slider and bouncing vibration in near-contact regime. *IEEE T MAGN* **40**(4): 136–3141 (2004)

[5] Ono K, Yamane M, Yamaura H. Experimental and analytical study of bouncing vibrations of a flying head slider in a near-contact regime. *J Tribol* **127**(2): 376–386 (2005)

[6] Yoon Y, Talke F E. Touch-down and take-off hysteresis of magnetic recording sliders on discrete track media. *Microsyst Technol* **16**(1–2): 273–278 (2010)

[7] Thornton B H, Bogy D B. Head–disk interface dynamic instability due to intermolecular forces. *IEEE T Magn* **39**(5): 2420–2422 (2003)

[8] Guo Q, Chung P S, Jhon M S. Nano-mechanics of perfluoropolyether films: Compression versus tension. *IEEE T Magn* **44**(11): 3698–3701 (2008)

[9] Liu X J, Amemiya K, Wong C H, Yu S K, Liu B. Molecular study of dynamic behavior between head and ultrathin lubricant film. *J Adv Mech Des Syst* **4**(1): 56–60 (2010)

[10] Suk M. Effect of tribocharging on lubricant redistribution. *IEEE T Magn* **41**(2): 831–835 (2005)

[11] Wang Y, Wei X F, Liang X H, Yin S Y, Zi Y Y, Peng Y Z, Tsui K L. The instability of angstrom-scale head–disk interface induced by electrostatic force. *IEEE T Magn* **51**(11): 3301304 (2015)

[12] Knigge B E, Mate C M, Ruiz O, Baumgart P M. Influence of contact potential on slider–disk spacing: Simulation and experiment. *IEEE T Magn* **40**(4): 3165–3167 (2004)

[13] Trinh T D, Spada F E, Ovcharenko A,Talke F E. Investigation of the contact potential of the head–disk interface using Kelvin probe measurements. In: Proceedings of the ASME–JSME 2018 Joint International Conference on Information Storage and Processing Systems and Micromechatronics for Information and Precision Equipment, San Francisco, USA, 2018: V001T01A008.

[14] Suh A Y, Polycarpou A A. Adhesive contact modeling for sub-5-nm ultralow flying magnetic storage head–disk interfaces including roughness effects. *J Appl Phys* **97**(10): 104328 (2005)

[15] Zheng J L, Bogy D B. Numerical simulation of touchdown dynamics of thermal flying-height control sliders. *IEEE T Magn* **48**(9): 2415–2420 (2012)

[16] Rajauria S, Ruiz O, Canchi S V, Schreck E, Dai Q. Electrostatically tunable adhesion in a high speed sliding interface. *Phys Rev Lett* **120**(2): 026101 (2018)

[17] Hughes B D, White L R. Analytic approximations for the elastic contact of rough spheres. *J Appl Mech* **47**(1): 194–196 (1980)

[18] Greenwood J A, Williamson J B P. Contact of nominally flat surfaces. *P Roy Soc A-Math Phy* **295**(1442): 300–319 (1966)

[19] Lee S C, Polycarpou A A. Microtribodynamics of pseudo-contacting head–disk interfaces intended for 1 Tbit/in^2. *IEEE T Magn* **41**(2): 812–818 (2005)

[20] Stanley H M, Etsion I, Bogy D B. Adhesion of contacting rough surfaces in the presence of sub-boundary lubrication. *J Tribol* **112**(1): 98–104 (1990)

[21] Kogut L, Etsion I. A static friction model for elastic-plastic contacting rough surfaces. *J Tribol* **126**(1): 34–40 (2004)

[22] Lee S C. Microtribodynamics of sub-five nanometers flying head–disk interfaces in magnetic storage. Ph.D. Thesis. Champaign–Urbana (USA): University of Illinois at Urbana–Champaign, 2004.

[23] Chang W R, Etsion I, Bogy D B. An elastic–plastic model for the contact of rough surfaces. *J Tribol* **109**(2): 257–263 (1987)

[24] Mitchell J P. Particles on surfaces 1: Detection, adhesion and removal. *J Aerosol Sci* **22**(2): 229 (1991)

[25] Wang Y, Zhao Y P. Electrowetting on curved surfaces. *Soft Matter* **8**(9): 2599–2606 (2012)

[26] Tani H, Mitsutome T, Kamei D, Tagawa N. Relationship of adhesion/friction forces and slider vibration in surfing–recording HDI system. *IEEE T Magn* **49**(7): 3752–3755 (2013)

[27] Ono K, Yamane M. Improved analysis of unstable bouncing vibration and stabilizing design of flying head slider in near-contact region. *J Tribol* **129**(1): 65–74 (2007)

[28] Li N, Zheng L S, Meng Y G, Bogy D B. Experimental study of head–disk interface flyability and durability at sub-1-nm clearance. *IEEE T Magn* **45**(10): 3624–3627 (2009)
[29] Wang Y, Wei X F, Liang X H, Yin S Y, Zi Y Y, Tsui K L. An *in situ* measurement method for electric potential at head–disk interface using a thermal asperity sensor. *IEEE T Magn* **52**(1): 3300106 (2016)
[30] Zheng J L, Bogy D B. A numerical investigation of different touchdown patterns of thermal-flying-height-control sliders. *Microsyst Technol* **19**(9–10): 1377–1381 (2013)

Fan ZHANG. He received his B.S. degree in mechanical engineering from Chongqing University, Chongqing, China. He is currently pursuing his Ph.D. degree from Xi'an Jiaotong University, Xi'an, China. His research interests include dynamics of sub-nanometer interface and material wear of the head at sub-nanometer interface.

Yu WANG. He received his Ph.D. degree in systems engineering and engineering management from City University of Hong Kong, Hong Kong, China, in 2014. He is currently an associate professor at School of Mechanical Engineering, Xi'an Jiaotong University, Xi'an, China. His current research interests cover dynamics of sub-nanometer interface, reliability assessment, and fault prognostics.

Yueqiang HU. He received his Ph.D. degree in mechanical engineering from Tsinghua University, Beijing, China, in 2018. He joined College of Mechanical and Vehicle Engineering, Hunan University, Changsha, China, in 2018. His current position is an associate professor. His research areas cover the nanofabrication and surface/interface science.

Mingquan ZHANG. He received his Ph.D. degree from Xi'an Jiaotong University, Xi'an, China, in 2019. His current research interests include mechanical equipment condition monitoring, fault diagnosis, signal processing, dynamic modeling, digital twin, health management, and system reliability.

Baotong LI. He received his Ph.D. degree from Xi'an Jiaotong University, Xi'an, China. He is currently a professor at School of Mechanical Engineering, Xi'an Jiaotong University, Xi'an, China. He once won the National Science Fund for Outstanding Young Scholars, China. His research focuses on the large-scale intelligent computing, energy finite element, equal geometric design, and structural topology optimization.